Journal of Alloys and Compounds 635 (2015) 136–141

Contents lists available at ScienceDirect

Journal of Alloys and Compounds

journal homepage: www.elsevier.com/locate/jalcom

Site selective spectroscopy in $BaYF_5:RE^{3+}$ (RE = Eu, Sm) nano-glass–ceramics

J. del-Castillo [a,*], A.C. Yanes [a], S. Abe [b,c], P.F. Smet [b,c]

[a] Dpto. Física, Universidad de La Laguna, 38206 La Laguna, Tenerife, Spain
[b] LumiLab, Department of Solid State Sciences, Ghent University, Krijgslaan 281-S1, 9000 Gent, Belgium
[c] Center for Nano- and Biophotonics (NB Photonics), Ghent University, Belgium

ARTICLE INFO

Article history:
Received 19 December 2014
Received in revised form 24 January 2015
Accepted 27 January 2015
Available online 12 February 2015

Keywords:
$BaYF_5$ nanocrystals
Rare-earth ions
Sol–gel method
Glass–ceramics
Luminescence

ABSTRACT

Trivalent rare-earth (RE = Eu, Sm) doped transparent nano-glass–ceramics comprising $BaYF_5$ nanocrystals were successfully obtained by appropriate heat-treatment of the corresponding precursor sol–gel glasses. Their structural and spectroscopic properties were investigated and compared with those for Eu^{3+}-doped-$BaYF_5$ nanocrystals prepared by a solvothermal method. X-ray Diffraction, Transmission Electron Microscopy and Energy Dispersive X-ray Spectroscopy measurements confirmed the distribution of $BaYF_5$ nanocrystals in the glass matrix, presenting a cubic phase structure with space group *Fm-3m*. In order to achieve a further structural characterization, the luminescence properties of the Eu^{3+} and Sm^{3+} dopants were also used as sensitive probes. The reduction in the emission intensities of hypersensitive transitions $^5D_0 \rightarrow {}^7F_2$ and $^4G_{5/2} \rightarrow {}^6H_{9/2}$ for Eu^{3+} and Sm^{3+} ions respectively, along with time-resolved measurements, confirm the distribution of a significant fraction of RE ions into the fluoride nanocrystal environment. These results suggest that $BaYF_5$ nano-glass–ceramics doped with Eu^{3+} or Sm^{3+} can be considered as potential red-emitting phosphors for the development of white LEDs under near UV excitation.

1. Introduction

The interest in rare-earth (RE) doped low-phonon energy nanomaterials has grown in recent decades due to their promising applications in light-emitting devices, biological labelling and imaging, up-conversion (UC) lasers, high density memories, among others [1,2]. In particular, RE doped oxyfluoride nano-glass–ceramics (nGCs) have attracted attention due to the mechanical and chemical properties of oxide glasses [3] and the lower phonon energies encountered in fluorides, which means that non-radiative quenching of emission is limited and therefore higher efficiencies can be reached. Thus, the nGCs present a high degree of transparency, due to the small nanocrystals (NCs) being dispersed in a transparent matrix (e.g. silica). In addition, energy transfer (ET) processes between neighbouring RE ions are favoured for the shortening of their interionic distances in the precipitated NCs. In this sense, the distribution of the optically active RE ions into the fluoride environment is of particular interest in view of the luminescent properties.

There is a large collection of reported work on fluorides such as $AREF_4$, MF_2, REF_3 and xMF_2–$yREF_3$ (A = alkali metal ions, M being a group-II element) [4–15]. MF_2–REF_3 systems have been extensively investigated and used as good host matrix for many optically active ions, with application in laser crystals and as UC material [16]. In this sense, $BaYF_5$ is an interesting host material due to its structure and optical properties [17–19], being transparent in a large electromagnetic domain and with a low maximum phonon frequency, leading to a potentially large number of emitting levels. Although there is an extensive literature on RE doped-$BaYF_5$ NCs [17–20], only a few about nGCs comprising $BaYF_5$ NCs were reported [21–25]. These $BaYF_5$ nGCs can be obtained from low cost and non-poisonous BaF_2, YF_3 and Y_2O_3 raw materials using the conventional thermal quenching method [26], however the volatilization at high melting temperature is problematic. An improvement in the nGCs preparation is achieved by using the sol–gel technique, allowing the formation of the precursor glasses at room temperature, and their corresponding nGCs at comparatively lower temperatures. Thus, by avoiding the evaporation losses, it is possible to precisely control the nGCs' chemical composition [27]. Moreover, the RE ions can be introduced into the "sol" giving rise to an excellent homogeneity in the final material, in contrast to common diffusion driven solid state reactions.

Within the large set of RE ions, the red emission of Eu^{3+} was essential in the development of (compact) fluorescent lights and

* Corresponding author.
E-mail address: fjvargas@ull.edu.es (J. del-Castillo).

http://dx.doi.org/10.1016/j.jallcom.2015.01.244
0925-8388/

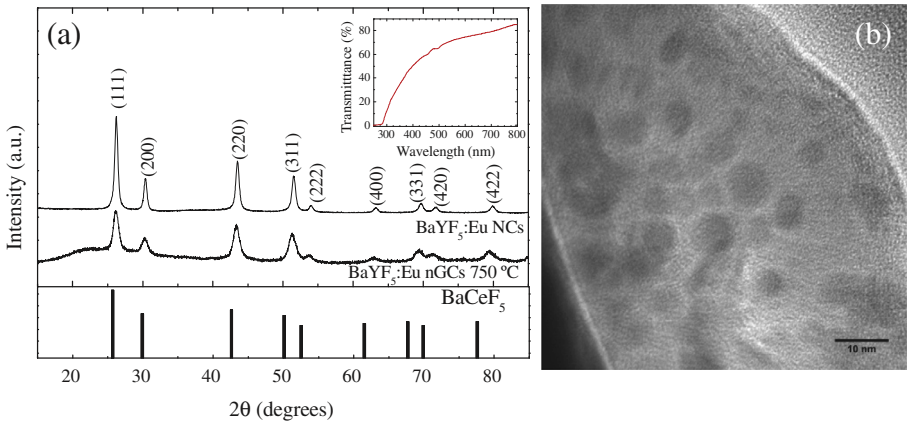

Fig. 1. (a) XRD patterns of Eu^{3+} doped-$BaYF_5$ nGCs and Eu^{3+} doped-$BaYF_5$ NCs. Standard peaks of $BaCeF_5$ (JCPDS 43-0394) are included for comparison. Inset shows the transmittance curve of Eu^{3+} doped-$BaYF_5$ nGCs. (b) TEM image of the Eu^{3+} doped-$BaYF_5$ nGCs heat treated at 750 °C.

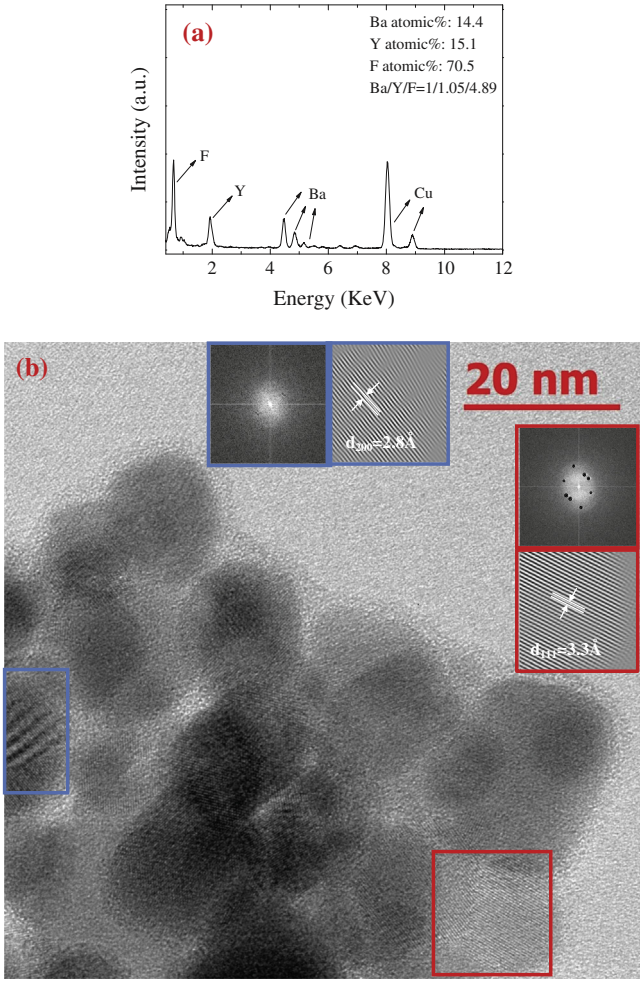

Fig. 2. (a) EDX spectrum of Eu^{3+} doped-$BaYF_5$ NCs. (b) Corresponding HRTEM image. Insets show power spectrum (FFT pattern) and filtered higher-contrasted image of red and blue squared nanoparticles. (For interpretation of the references to colour in this figure legend, the reader is referred to the web version of this article.)

cathode ray tubes, as it offers a great return in luminous efficacy, due to the narrow-banded emission in the red part of the visible spectrum where the eye sensitivity is still relatively high. However, Eu^{3+} ions are in principle not a good choice for use in LED conversion phosphors, due to the low absorption strength of the 4f–4f transitions in Eu^{3+} in the near-UV to blue region. To obtain sufficiently high absorption strength, there are basically two options. First, a Eu^{3+} based phosphor can be processed into a dense, pore-free ceramic disk, in which the absorption can be enhanced, while keeping scattering losses low [28]. However, it is often not straightforward or cost-effective to convert common powder phosphors into high density ceramic platelets. The second option is pursued in this work, where a Eu^{3+} containing luminescent NC is naturally embedded in a transparent matrix. In this way, scattering due to a mismatch of the refractive index is avoided when the NCs are sufficiently small.

In this work we present for the first time, as far as we know, sol–gel derived nGCs containing Eu^{3+} or Sm^{3+} doped-$BaYF_5$ NCs. A complete structural analysis has been carried out, leading to the assignment of the $BaYF_5$ crystalline phase as cubic. In literature at least two different assignments can be found, related to tetragonal and cubic phases of $BaYF_5$ [29 and refs therein]. A major issue for NCs embedded in nGCs is the incorporation of the dopant ions. For this, the local environment of RE ions can be analysed taking into account their luminescent features. In some cases transition probabilities are especially sensitive to the local symmetry, and therefore can be used as probe ions. In the case of Eu^{3+} and Sm^{3+} ions, the electric dipole (ED) character of hypersensitive transitions $^5D_0 \rightarrow {}^7F_2$ and $^4G_{5/2} \rightarrow {}^6H_{9/2}$ respectively, presents high sensitivity to the local environment [30]. Thus, by using Eu^{3+} and Sm^{3+} it is possible to discern between crystalline and glassy environments by means of site-selective spectroscopy and time-resolved measurements, especially if the crystalline host contains centrosymmetric sites. Moreover, Eu^{3+} doped-$BaYF_5$ NCs were successfully obtained by a solvothermal method in order to compare and confirm the cubic structure of fluoride NCs in the nGCs system.

2. Experimental

Silica glasses with a composition consisting of $95SiO_2$–$5BaYF_5$ doped with 0.1 of Eu^{3+} or Sm^{3+} ions (in mol%) were obtained by sol–gel method in a similar way as described in Ref. [31]. Tetraethoxysilane (TEOS) $Si(OCH_2CH_3)_4$, used as a source of SiO_2, was hydrolysed for 1 h at room temperature with a mixed solution of ethanol and deionized H_2O, using acetic acid as a catalyst. The molar ratio of TEOS:ethanol:H_2O:CH_3COOH was 1:4:10:0.5. As sources of Ba and Y, $Ba(CH_3COO)_3 \cdot xH_2O$ and $Y(CH_3COO)_3 \cdot xH_2O$ were used. The required quantities of $Ba(CH_3COO)_3 \cdot xH_2O$, $Y(CH_3COO)_3 \cdot xH_2O$, $Eu(CH_3COO)_3 \cdot xH_2O$ and $Sm(CH_3COO)_3 \cdot xH_2O$ were dissolved in a CF_3COOH and H_2O solution, which were slowly mixed with the initial solution. The molar ratio of metal ions to CF_3COOH was 1:5. In order to make the solution homogeneous, it was stirred vigorously for 1 h at room temperature. A highly transparent gel was obtained by leaving the resultant homogeneous solution in a sealed container at 35 °C for several days. The gels were then dried by slow evaporation for approximately four weeks to remove residual water and solvents. Finally, these sol–gel glasses were heat-treated in an air atmosphere at 750 °C in order to achieve the controlled precipitation of $BaYF_5$ nanocrystals, required to produce transparent nGCs.

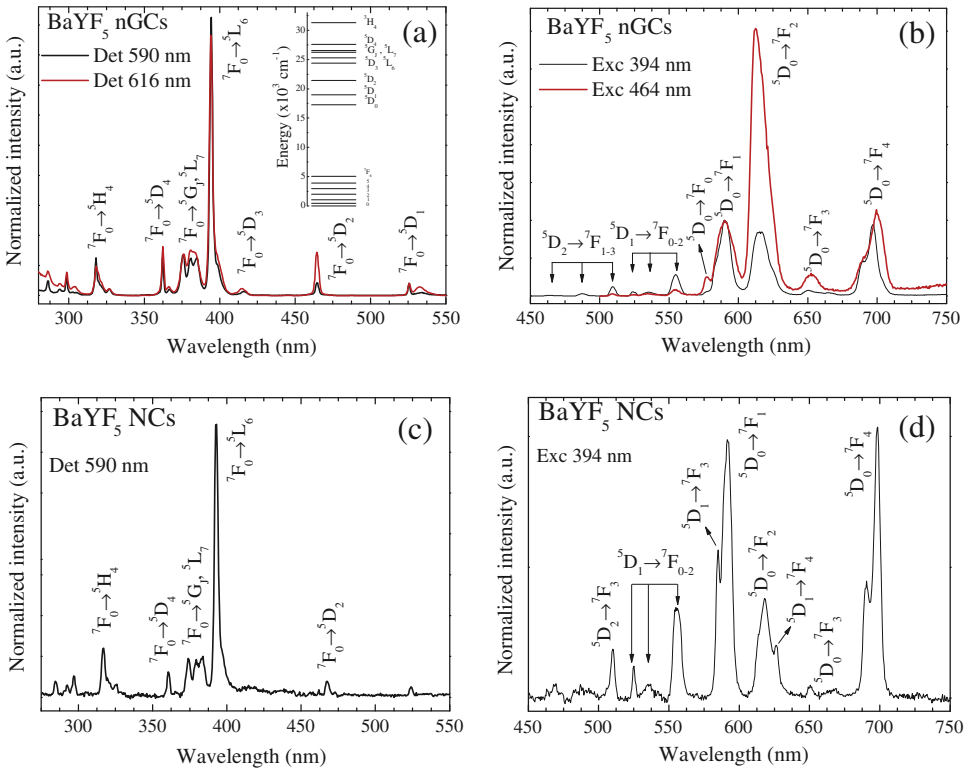

Fig. 3. Excitation (a) and emission (b) spectra of Eu^{3+} doped-$BaYF_5$ nGCs detecting and exciting at indicated wavelengths. Corresponding excitation (c) and emission (d) spectra of Eu^{3+} doped-$BaYF_5$ NCs, detecting and exciting at indicated wavelengths.

Moreover, $BaYF_5$ NCs doped with 2% of Eu^{3+} ions were prepared through a solvothermal method using oleic acid as capping ligand to control the particle growth and prevent the NCs from aggregation, as described in Refs. [2,29]. In brief, 2 ml deionized H_2O, 0.6 g NaOH, 10 ml ethanol and 20 ml oleic acid were mixed together under vigorous stirring to form a transparent homogeneous solution. Then, an aqueous solution (4 ml) of $Ba(NO_3)_2$ (0.5 mmol) and a stoichiometric amount of $Y(NO_3)_3$, $Eu(NO_3)_3$ were added to above solution. After that, 1 ml of aqueous solution containing 2.5 mmol NH_4F was added. After stirring for another 20 min, the as-obtained homogeneous colloidal solution was transferred into a 50 ml stainless Teflon-lined autoclave and kept at 200 °C for 24 h. The autoclave was naturally cooled down to room temperature. The precipitate deposited at the bottom of Teflon vessel was collected by centrifugation, washed with ethanol and deionized water several times, and then dried in air at 60 °C for 24 h. The obtained NCs were dispersed in toluene (2 wt%) for all spectroscopic measurements.

Powder X-ray Diffraction (XRD) patterns of the samples were recorded with a Philips X'Pert Pro diffractometer equipped with a primary monochromator, a Cu $K_{\alpha 1 \alpha 2}$ radiation source, and an X'Celerator detector. The XRD patterns were collected with a step of 0.016° in the 2θ angular range from 15° to 85° and an acquisition time of 2 h. Furthermore, the diffraction pattern of LaB_6 was used as an internal standard to calibrate the parameters of the instrument profile. Transmission Electron Microscopy (TEM-HRTEM) images were obtained using a JEOL 2200FS microscope operating at 200 kV, equipped with a Field Emission Gun, which allowed us to achieve a point-to-point resolution of 0.17 nm. Samples were prepared by dispersing fine powder, obtaining by grinding the samples, in ethanol and dropping them onto carbon-coated copper grids. Selected areas of the HRTEM images were mathematically filtered by means of Fast Fourier Transform (FFT) analysis resulting in Power Spectra patterns, corresponding to the eigen-frequencies of the observed NCs. Further, the relevant frequencies were selected to filter the noise in the zoomed areas of the HRTEM images and to produce higher contrast images of the atomic planes of the observed NCs.

Transmittance of nGCs was measured by means of a Perkin–Elmer Lambda 9 ultraviolet–visible infrared (UV–Vis-IR) spectrophotometer with a resolution of 0.5 nm.

Luminescence measurements were performed using an Edinburgh Instruments' FLS920 fluorescence spectrometer, with a 0.3 m double excitation monochromator and an 0.3 m emission monochromator, to record the emission spectra in the wavelength range of 200–850 nm (with a Hamamatsu R928 photomultiplier tube). The time resolved photoluminescence measurements were carried out using a PTI spectrometer, where a 75 W Xenon flash lamp acts as excitation source. All spectra were collected at room temperature and corrected for the instrumental response.

3. Results and discussion

The structural characterization was carried out by means of XRD patterns and TEM and HRTEM images. Fig. 1(a) presents the XRD pattern of $BaYF_5$ nGCs doped with 0.1 Eu^{3+} (mol%), showing a broadband characteristic of the SiO_2 along with diffraction peaks at 26.3°, 30.4°, 43.5°, 51.5°, 53.9°, 63.2°, 69.7°, 71.8° and 79.8° in 2θ range from 15° to 85°. By using the strongest peak at 2θ = 26.3° and the Scherrer equation, a mean NCs size of 11 nm was obtained. This value is in a reasonably good agreement with the size observed by TEM imaging, Fig. 1(b), where the NCs are visible as dark spots, dispersed in the amorphous silica network of the nGC system. Moreover, they are appreciably smaller than those obtained previously in $BaYF_5$ nGCs by Biswas et al. [21] around 30–50 nm, Huang et al. [22] and Gu et al. [23] around 11–31 nm and Liu et al. [24] around 25 nm. The $BaYF_5$ nGCs show high transparency, as can be seen in the inset of Fig. 1(a).

In order to confirm the presence of $BaYF_5$ NCs in the nGC system, Eu^{3+}-doped $BaYF_5$ NCs were prepared by solvothermal method. By using Energy Dispersive X-ray Spectroscopy (EDX) analysis in the as-prepared material, see Fig. 2(a), it is possible to determine its real composition. Peaks corresponding to Ba, Y and F are observed along with Cu and C peaks originating from the copper grid. The atomic ratios of Ba/Y/F are 1/1.05/4.89, which is in excellent agreement with the theoretical atomic Ba/Y/F ratio of 1/1/5 in $BaYF_5$ taking the accuracy of EDX spectroscopy into account.

Corresponding XRD pattern of Eu^{3+}-doped $BaYF_5$ NCs is also included in Fig. 1(a). All XRD peaks, in $BaYF_5$ nGCs and also in the $BaYF_5$ NCs, can be assigned to the cubic structure of $BaYF_5$ [17] similar to the standard peaks of $BaCeF_5$ (JCPDS 43-0394, space group *Fm-3m*), also shown in Fig. 1(a) for comparison. There is a slight shift in all XRD peaks to higher 2θ side, due to the possible

variation of the cell parameter related to the radius of Y^{3+} ions [8]. Thus, taking initially the structure of $BaCeF_5$ in a Rietveld refinement, we can estimate the lattice constant value of $a = 5.853$ and 5.879 Å, for $BaYF_5$ nGCs and NCs, respectively, in a good agreement with previous results [17,29].

Next, to complete the structural characterization, HRTEM images were collected for the Eu^{3+}-doped $BaYF_5$ NCs. The observed NCs in the HRTEM bright-field micrograph are clearly distinguished as dark particles, see Fig. 2(b), with mean size around 20–30 nm. This is comparable with the size estimated by the Scherrer equation (around 30 nm). The power spectrum from the squared NCs lead us to obtain filtered images by using the frequencies determined from the FFT pattern, see insets in Fig. 2(b). The interplanar distances of 3.34 and 2.88 Å correspond to (1 1 1) and (2 0 0) planes of $BaYF_5$ cubic phase respectively. The results from HRTEM analysis are consistent with the previously analysed XRD data.

Most trivalent RE ions show visible or infrared emissions, due to electron transitions within the $4f^n$ electronic configurations. Because the 4f electrons are well shielded from the crystal environment, the emission and excitation peaks are relatively narrow. Besides the use of lanthanide ions for luminescence based applications, the dependency of the relative intensity of certain transitions, as well as their lifetime and multiplet splitting, can be used as a probe for the local environment of the RE ions.

The luminescent features of Eu^{3+} and Sm^{3+} ions could therefore reveal whether the RE ions are actually incorporated in the NCs or distributed in the nGCs, outside the NCs. Fig. 3(a and b) shows excitation and emission spectra of the $BaYF_5$ nGCs doped with 0.1Eu^{3+} (mol%), detecting and exciting at the indicated wavelengths. For the excitation, spectra have been normalized at the maximum of the intensity at 525 nm ($^7F_0 \rightarrow {}^5D_1$), because this transition is weakly dependent on the local environment of the Eu^{3+} ions. These spectra present mainly excitation peaks of Eu^{3+} ions corresponding to transitions from $^7F_0$ ground level to the excited levels labelled in the figure, according the energy level diagram included in the inset of Fig. 3(a). In particular, the $^7F_0 \rightarrow {}^5D_2$ transition (around 464 nm) shows electric dipole character (ED), hypersensitive to the local structure around Eu^{3+} ions, and therefore forbidden in the centrosymmetric environments. Thus, by detecting the emission $^5D_0 \rightarrow {}^7F_1$ at 590 nm (with magnetic dipole character MD) or the $^5D_0 \rightarrow {}^7F_2$ at 616 nm (with electric dipole character ED), insensitive and hypersensitive to the crystal field environment for the Eu^{3+} ions respectively, significant differences can be observed. The intensity of the excitation peak corresponding to the transition $^7F_0 \rightarrow {}^5D_2$ at 464 nm, is diminished when detecting at 590 nm instead of 616 nm. This result along with a better resolved Stark structure of the excitation bands below 380 nm can be related with a more crystalline environment for the Eu^{3+} ions.

On the other hand, the emission spectra upon excitation at 394 and 464 nm have been normalized at the maximum of the ($^5D_0 \rightarrow {}^7F_1$) transition at 590 nm, with MD character, which is non-sensitive to local site symmetry, see Fig. 3(b). Upon excitation at around 394 nm, emissions originating from the $^5D_2$, $^5D_1$ and $^5D_0$ levels are observed, which can be related with a low-phonon-energy environment for Eu^{3+} ions. However, by exciting at 464 nm (i.e. promoting the excitation of Eu^{3+} ions with low symmetry), the relative intensity of all emissions reduces and, in particular the emissions coming from upper-lying $^5D_2$ and $^5D_1$ levels almost disappear, related with glassy environments that present higher phonon energy. To clarify this assumption, we used the asymmetry ratio R defined as the ratio between the ED $^5D_0 \rightarrow {}^7F_2$ to MD $^5D_0 \rightarrow {}^7F_1$ transitions. This ratio can be useful as a measurement of how close the local environment is to centrosymmetric [30,32]. In this case, R value of 0.8 was obtained when exciting at 394 nm which confirms that the environment of Eu^{3+} ions gets closer to a centrosymmetric site, related with their distribution into the $BaYF_5$ NCs. On the contrary, exciting at 464 nm, R value of 3.5 is obtained, associated with a non-centrosymmetric environment for Eu^{3+} ions that remain in the silica glassy phase.

Next, we analyse the excitation and emission spectra of Eu^{3+} doped-$BaYF_5$ NCs, where similar luminescent features should be expected. Thus, the excitation spectrum, see Fig. 3(c), shows well-resolved excitation peaks of Eu^{3+} ions, similar to the peaks previously observed in the $BaYF_5$ nGCs detecting at 590 nm. It should be noticed that the intensity of the $^7F_0 \rightarrow {}^5D_2$ excitation peak at 464 nm also diminishes when comparing with the excitation spectrum of the $BaYF_5$ nGCs detecting at 616 nm (glassy environment). The corresponding emission spectrum, see Fig. 3(d), shows, besides the characteristic emissions from the $^5D_0$ level, emission peaks from the $^5D_2$ and $^5D_1$ levels, which are more significant than those observed in the nGCs system when exciting at the same wavelength, which is related with a lower-phonon energy environment for the Eu^{3+} ions. The lower R value of 0.4 for Eu^{3+} doped-$BaYF_5$ NCs when comparing with the corresponding one in the nGCs, (R value = 0.8) can be explained by the higher symmetry environment for the Eu^{3+} ions. These results are in good agreement with a larger NC size as it was observed by XRD and HRTEM measurements.

Furthermore, to confirm the previously observed differences between crystalline and glassy environments for Eu^{3+} ions in the $BaYF_5$ nGCs, time-resolved photoluminescence measurements were carried out in the nGCs system and in the NCs. In this sense, the behaviour of the luminescence decay from the $^5D_0$ level was measured, selecting the excitation and detection wavelengths corresponding to the different sites previously observed. Fig. 4 shows time-resolved photoluminescence decays for $BaYF_5$ nGCs, exciting at 464 nm and detecting the 616 nm emission (corresponding to a glassy environment), and exciting at 394 nm and detecting the 590 nm emission (corresponding to a close to inversion symmetry site associated to nanocrystalline $BaYF_5$ environment). In the first case, an effective lifetime value of 1.63 ms related to the amor-

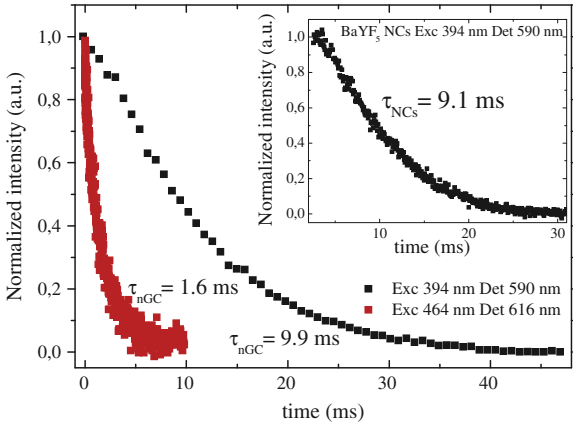

Fig. 4. Time-resolved photoluminescence measurements of a Eu^{3+} doped-$BaYF_5$ nGCs exciting at 394 nm and monitoring at 590 nm ($BaYF_5$ nGCs nanocrystalline environment) and exciting at 464 nm and monitoring the 616 nm ($BaYF_5$ nGCs glassy environment). Inset shows time-resolved photoluminescence measurements of Eu^{3+} doped-$BaYF_5$ NCs exciting at 394 nm and monitoring at 590 nm.

Table 1
Effective lifetime values of Eu^{3+} doped-$BaYF_5$ nGCs and Eu^{3+} doped-$BaYF_5$ NCs.

	τ_{eff} (ms)
$BaYF_5$ nGCs Exc 394 nm Det 590 nm	9.88 ± 0.19
$BaYF_5$ nGCs Exc 464 nm Det 613 nm	1.63 ± 0.03
$BaYF_5$ NCs Exc 394 nm Det 590 nm	9.12 ± 0.14

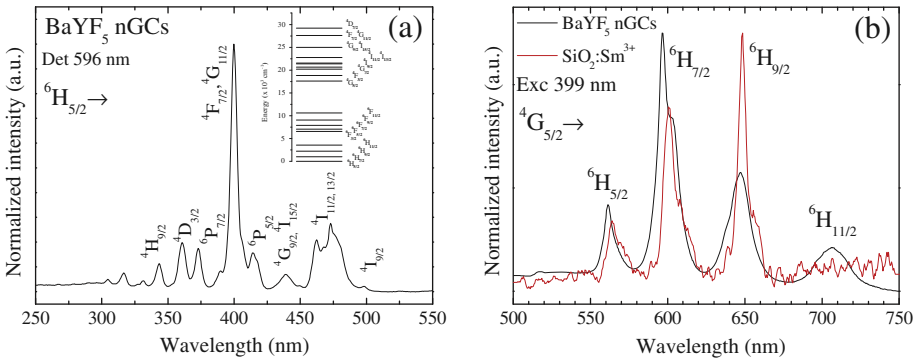

Fig. 5. Excitation (a) and emission (b) spectra of Sm^{3+} doped-$BaYF_5$ nGCs detecting and exciting at indicated wavelengths. Emission spectrum of Sm^{3+} ions in silica glassy environment has also been included for comparison [34].

phous environment of Eu^{3+} ions in the glass phase is obtained from the area under the curve through the expression $\tau_{eff} = \int_0^\infty I(t)dt/I(0)$, see Table. 1. However in the second case, a value of 9.88 ms that can be related with Eu^{3+} ions distributed inside the $BaYF_5$ NCs, is obtained. To confirm this assumption, a value of 9.12 ms, similar to the previous one obtained in the nGCs, was obtained in the Eu^{3+}-doped $BaYF_5$ NCs, exciting at 394 nm and detecting at 590 nm. The limited deviation from a single exponential decay profile might be related to energy migration between Eu^{3+} ions or to variations in the local coordination of the dopant ions. Although it would be interesting to study the different spectral contributions in the decay profile in more detail, the analysis is further complicated by the feeding from the higher $^5D_1$ level, as observed in the initial part of the decay profile.

Finally, in order to complete the structural analysis we also study the luminescence features of the Sm^{3+}-doped $BaYF_5$ nGCs. In a similar way than Eu^{3+} ions, Sm^{3+} ions can also act as a spectroscopic probe of the local structure around RE ions. This is related with the ED character of the $^4G_{5/2} \rightarrow {}^6H_{9/2}$ hypersensitive transition, for which the intensity increases as the symmetry of the local environment of the luminescent site decreases [33]. The excitation spectrum of the Sm^{3+}-doped $BaYF_5$ nGCs, obtained by detecting the 596 nm emission, corresponding to the $^4G_{5/2} \rightarrow {}^6H_{7/2}$ transition, presents peaks arising from the ground state $^6H_{5/2}$ to excited levels labelled in Fig. 5(a) according to its energy level diagram. The corresponding emission spectrum upon excitation at the most intense excitation peak, at 399 nm, is presented in Fig. 5(b) showing four main emissions in the yellow-to-red part of the visible spectrum coming from the $^4G_{5/2}$ level. On the other hand in SiO_2–SnO_2 nGCs doped with Sm^{3+} ions, previously studied by authors [34], the relative intensities of these emission peaks are markedly different when Sm^{3+} ions remain in silica glassy environment, see Fig. 5(b). Similar to the case of Eu^{3+} ions, the intensity ratio R between the $^4G_{5/2} \rightarrow {}^6H_{9/2}$ (ED character, hypersensitive to the local environment) to $^4G_{5/2} \rightarrow {}^6H_{5/2}$ (predominant MD character, insensitive to the local environment) emission transitions for Sm^{3+} was calculated. The R values of 1.4 and 3.7 were obtained for the Sm^{3+}-doped $BaYF_5$ nGCs and Sm^{3+} ions remaining in the silica glassy environment, respectively, indicating that the environment of Sm^{3+} ions in the nGCs system is close to an inversion symmetry site. Moreover, by comparing both emission spectra, a blue-shift in the Sm^{3+}-doped $BaYF_5$ nGCs sample can be observed, which is related to an effect of the different crystal field in both types of environments.

Therefore, all shown results suggest that an important fraction of RE ions is incorporated into the $BaYF_5$ NCs in both studied nGCs systems. This is supported by the fact that both ions (Eu^{3+} and Sm^{3+}) can occupy the Y^{3+} sites with similar ionic radius, without the need for charge compensation, thus increasing the RE solubility. This leads to the conclusion that these nGCs systems are promising candidates as red-emitting phosphors in white LEDs.

4. Conclusions

The successful development of sol–gel transparent nGCs, comprising Eu^{3+} or Sm^{3+}-doped $BaYF_5$ NCs, after adequate heat treatments of the corresponding precursor glasses was achieved. The precipitation into a SiO_2 matrix of $BaYF_5$ NCs with an estimated size of 11 nm was confirmed by XRD and TEM images. In order to further confirm the presence of cubic $BaYF_5$ NCs in the nGC system, Eu^{3+}-doped $BaYF_5$ NCs were prepared by solvothermal method and their luminescent properties were studied and compared with the Eu^{3+}-doped nGCs. Moreover, the use of Eu^{3+} and Sm^{3+} as probe ions in the nGCs led us to distinguish between amorphous and like-crystalline environments and confirm the incorporation of a large fraction of RE ions into the $BaYF_5$ NCs. These results suggest that $BaYF_5$ nGCs doped with Eu^{3+} or Sm^{3+} can be considered as potential red-emitting phosphors for the development of white LEDs under near UV excitation.

Acknowledgements

The authors are grateful for financial support to Fundación CajaCanarias – Spain (NAFOWLEDs) and IWT – Belgium (Flemish agency for Innovation by Science and Technology) through the SBO-project LumiCoR (IWT 130030). J. del-Castillo would like to thank Ghent University for his mobility grant and, in particular, the hospitality of LumiLab members during his stay in Ghent.

References

[1] W. Niu, S. Wu, S. Zhang, L. Li, Chem. Commun. 46 (2010) 3908.
[2] M. Wang, C.C. Mi, W.X. Wang, C.H. Liu, Y.F. Wu, Z.R. Xu, C.B. Mao, S.K. Xu, ACS Nano 3 (2009) 1580.
[3] D.Q. Chen, Y.S. Wang, F. Bao, Y.L. Yu, J. Appl. Phys. 101 (2007) 113511.
[4] K. Zheng, D. Zhao, D. Zhang, N. Liu, F. Shi, W. Qin, J. Alloys Comp. 509 (2011) 5848.
[5] C.E. Secu, M. Secu, C. Guica, L. Mihut, Opt. Mater. 33 (2011) 1770.
[6] F. Xin, S. Zhao, G. Jia, L. Huang, D. Deng, H. Wang, S. Xu, Mater. Chem. Phys. 137 (2012) 177.
[7] J. del-Castillo, A.C. Yanes, A. Santana-Alonso, J. Méndez-Ramos, Opt. Mater. 37 (2014) 511.
[8] J.J. Velázquez, V.D. Rodríguez, A.C. Yanes, J. del Castillo, J. Méndez-Ramos, Appl. Phys. B 108 (2012) 577.
[9] A. Santana-Alonso, A.C. Yanes, J. Méndez-Ramos, J. del-Castillo, V.D. Rodríguez, Opt. Mater. 33 (2011) 587.
[10] J. del-Castillo, A.C. Yanes, J. Méndez-Ramos, V.K. Tikhomirov, V.V. Moshchalkov, V.D. Rodríguez, J. Sol–Gel Sci. Technol. 53 (2010) 509.
[11] T. Grzyb, M. Runowski, S. Lis, J. Lumin. 154 (2014) 479.
[12] J. Lin, J. Huo, Y. Cai, Q. Wang, J. Lumin. 144 (2013) 1.
[13] X. Changfu, M. Mo, Z. Songjun, R. Guozhong, Y. Liwen, Y. Qibin, J. Alloys Comp. 509 (2011) 7943.

[14] G. Lunjun, M. Mo, X. Changfu, L. Xujun, W. Suiping, L. Jianguo, Y. Qibin, J. Lumin. 134 (2013) 718.
[15] Y. Yu, Y. Wang, D. Chen, F. Liu, Ceram. Int. 34 (2008) 22143.
[16] X. Qiao, X. Fan, M. Wang, App. Phys. Lett. 89 (2006) 111919.
[17] Y. Huang, H. You, G. Jia, Y. Song, Y. Zheng, M. Yang, K. Liu, N. Guo, J. Phys. Chem. C 114 (2010) 18051.
[18] Y. Lei, M. Pang, W. Fan, J. Feng, S. Song, S. Danga, H. Zhang, Dalton Trans. 40 (2011) 142.
[19] H. Qiu, G. Chen, L. Sun, S. Hao, G. Han, C. Yang, J. Mater. Chem. 21 (2011) 17202.
[20] F. Vetrone, V. Mahalingam, J.A. Capobianco, Chem. Mater. 21 (2009) 1847.
[21] K. Biswas, A.D. Sontakke, K. Annapurna, Int. J. App. Glass Sci. 3 (2) (2012) 154.
[22] S. Huang, Q. Gao, M. Gu, J. Lumin. 132 (3) (2012) 750.
[23] M. Gu, Q.C. Gao, S.M. Huang, X.L. Liu, B. Liu, C. Ni, J. Lumin. 132 (10) (2012) 2531.
[24] F. Liu, Y. Wang, D. Chen, Y. Yu, E. Ma, L. Zhou, P. Huang, Mater. Lett. 61 (2007) 5022.
[25] Z. Shan, D. Chen, Y. Yu, P. Huang, F. Weng, H. Lin, Y. Wang, Mater. Res. Bull. 45 (2010) 1017.
[26] X. Qiao, X. Fan, M. Wang, H. Yang, X. Zhang, J. Appl. Phys. 104 (2008) 043508.
[27] C.J. Brinker, G.W. Scherer, Sol–Gel Science: The Physics and Chemistry of Sol–Gel Processing, Academic Press, Boston, 1990.
[28] P.F. Smet, A.B. Parmentier, D. Poelman, J. Electrochem. Soc. 158 (6) (2011) R37.
[29] M. Mo, Y. Liwen, R. Guozhong, X. Changfu, L. Jianguo, Y. Qibin, J. Lumin. 131 (2011) 1482.
[30] S. Cotton, Wiley, West Sussex, UK, 2006, pp. 14. (Chapter 2).
[31] A. Biswas, G.S. Maciel, C.S. Friend, P.N. Prasad, J. Non-Cryst Solids 316 (2003) 393.
[32] S. Fujihara, S. Koji, T. Kimura, J. Mater. Chem. 14 (8) (2004) 1331.
[33] A.C. Yanes, A. Santana-Alonso, J. Méndez-Ramos, J. del-Castillo, V.D. Rodríguez, Adv. Funct. Mater. 21 (2011) 3136.
[34] A.C. Yanes, J.J. Velázquez, J. del-Castillo, J. Méndez-Ramos, V.D. Rodríguez, Nanotechnology 19 (2008) 295707.